POLITECNICO DI TORINO
Repository ISTITUZIONALE

A novel test rig for friction parameters measurement on underplatform dampers

Original
A novel test rig for friction parameters measurement on underplatform dampers / Gastaldi, C., Berruti, T.M., Gola, M.M.. - In: INTERNATIONAL JOURNAL OF SOLIDS AND STRUCTURES. - ISSN 0020-7683. - ELETTRONICO. - 185-186:(2020), pp. 170-181. [10.1016/j.ijsolstr.2019.08.030]

Availability:
This version is available at: 11583/2786622 since: 2020-02-14T10:35:26Z

Publisher:
Elsevier Ltd

Published
DOI:10.1016/j.ijsolstr.2019.08.030

Terms of use:

This article is made available under terms and conditions as specified in the corresponding bibliographic description in the repository

Publisher copyright
Elsevier postprint/Author's Accepted Manuscript

© 2020. This manuscript version is made available under the CC-BY-NC-ND 4.0 license
http://creativecommons.org/licenses/by-nc-nd/4.0/.The final authenticated version is available online at:
http://dx.doi.org/10.1016/j.ijsolstr.2019.08.030

(Article begins on next page)

17 November 2026

A novel test rig for friction parameters measurement on underplatform dampers

C. Gastaldi[a,*], Teresa M. Berruti[a], Muzio M. Gola[a]

[a] *Politecnico di Torino, Corso Duca degli Abruzzi 24, 10129, Torino, Italy*

Abstract

The focus of this paper is on the direct experimental investigation of underplatform dampers, friction damping devices used on turbine bladed disks to limit resonant vibrations. Given the nonlinear and highly complex nature of dry friction, model validation of bladed disks with underplatform dampers still relies heavily on experimental verification, which is typically performed using the Frequency Response Function.

This paper is the authors' most recent effort to increase the understanding of friction and damper mechanics by gathering experimental evidence directly at the blade platform/damper interface.

A new test rig for frequencies and contact pressures in line with real working conditions has been developed. The geometry of the test rig and its technical features are described in detail in the paper. The dedicated experimental evidence thus obtained is used to estimate (not tune) contact parameters. The influence of frequency, centrifugal load and of the flat-on-flat contact interface morphology is highlighted. Results are compared with those gathered using similar dampers on a different test rig. Contact parameters are then be fed to a state-of-the-art numerical code for the prediction of the dynamic response of friction damped systems. The experimental-numerical comparison is used as validation and as a basis to investigate the simulation sensitivity to contact parameters variability.

*Corresponding author

Email address: chiara.gastaldi@polito.it (C. Gastaldi)

Keywords: friction, damping, turbine, contact stiffness, friction coefficient

Nomenclature

Symbols

CF	Centrifugal Force on the damper
k	Contact stiffness
β	Damper rotation
ΔF	Dynamic variation of the generic force component F, i.e. without the mean static component
μ	Friction coefficient
F	Generic Force
d	Generic in-plane displacement
u	Horizontal (≈tangent to the bladed disk) displacement
H	Horizontal (≈tangent to the bladed disk) force
N	Normal contact force
n	Normal displacement at the contact
T	Tangential contact force
t	Tangential displacement at the contact
w	Vertical (≈radial) displacement
V	Vertical (≈radial) force

Additional Subscripts

eq	Equivalent, referred to overall damper performance
L	Left damper-platform contact, i.e. flat-on-flat

R	Right damper-platform contact, i.e. cylinder-on-flat

Acronyms

FRF	Frequency Response Function
HBM	Harmonic Balance Method
IP	In Phase
OOP	Out of Phase
UPD	UnderPlatform Damper

1. Introduction

The dynamic design of turbine bladed disks has evolved over the years by including, in the dynamic numerical models, the friction dissipation due to the interfaces between different turbine elements. These elements can be integral part of the blades such as shrouds or interlocked tip platforms [1, 2, 3, 4, 5, 6, 7, 8, 9], or, as an alternative, they can be external devices such as underplatform dampers (UPDs) [10, 11, 12, 13, 14, 15, 16, 17, 18, 19].

The UPDs are metal masses inserted between the blades, pushed against the blade platforms by the centrifugal force. The design of UPDs has been extensively investigated in the past 15 years both as "solid dampers" in several shapes, i.e. cylindrical, curved flat, wedge [20, 21, 22, 23, 24, 25, 26, 27, 28], and as flexible dampers, namely strip dampers or seal dampers [29, 30, 31].

Experimental investigation in the field of friction damping prediction is usually performed for two main objectives:

- estimate contact parameters;
- gather experimental data (e.g. FRF response) to validate the results of numerical simulation tools.

These two objectives are typically pursued on different test rigs. The first objective is in most cases addressed through single contact test arrangements[32, 33, 34, 35, 36, 37]. However, the significant limitation of single contact test results is that they do not reveal the dependence of contact parameters on the real damper contact conditions.

The most common test rig architecture to tackle the second objective is composed by one damper placed between two blades excited with a shaker [19, 11, 38, 39, 40, 41, 42]. A modified architecture is used in [43, 44] in which two dampers are in contact with the different platforms of the same test blade. The other side of the damper is in contact with a stiffer structure called dummy blade. In [26] the dummy blade is substituted with force sensor to measure contact forces.

In all these experimental setups the centrifugal load acting on the damper is simulated by dead weights attached to the damper through wires and pulleys arrangement or solid strips. In a more complex test rig [15] a 24 blades assembly is excited with a rotating force to investigate the damper behavior at different nodal diameters of the disk. Dampers are loaded with dead weights as well. Dampers are loaded in a more realistic way if tests are performed using rotating disks[45, 16].

It is interesting to remark a growing interest in using damper kinematics as a means to better understand contact conditions. In [19] a laser measurement of damper kinematics is also introduced much in the way already adopted by AERMEC in 2010 [38] and used throughout its following papers [46, 47, 48, 49]. This signals a growing interest in improving the fidelity of damper modeling and to rigorously assess processes needed for reliable predictions.

However, all the previously cited experimental setups mainly study the overall effect of the damper on the blade in terms of vibration amplitude reduction and resonant frequency shift. This black-box like approach is functional to evaluate the capability of the damper to reduce resonant displacements but it does not allow a better understanding of the behavior of the damper, nor the estimation of its contact parameters.

What differentiates these authors' approach in damper testing is the will to add knowledge to the field by gathering direct experimental evidence at the damper-platform interface. The first Piezo Damper rig, first presented in [50] and fully described in [46] allows for platform displacements and forces to be directly measured; a laser arrangement is added that measures damper displacements and rotations, relating them to platform displacements and contact forces. This dedicated experimental evidence was, and still is, believed to be the most accurate way to determine contact parameters (tangential contact stiffness, friction coefficients).

In this paper the authors present a new test rig for the direct experimental investigation and contact parameter estimation of UPDs. As in the previous test rig [46], contact forces, damper rotation are directly measured by imposing a relative displacement at the two platforms. Unlike its predecessor it is now possible to reach frequencies and contact pressures in line with real UPDs working conditions. Furthermore, unlike single contact test arrangements, it unveils the influence of contact interface kinematics, normal load variation during the cycle, etc.

Section 2 gives a full description of the new test rig, while its experimental capabilities and a sample of results is shown in Sect. 3. Section 4 summarizes the contact parameter estimation procedure, with a particular focus on the tangential contact stiffness. Values extracted from different dampers are compared and checked for sample-to-sample variability. The influence of the contact surface configuration and that of imposed contact pressure are highlighted in Sect. 5. This contribution marks a definite improvement with respect to previous works[46]. The contact parameter thus derived are then fed to a state-of-the-art damper numerical model in Sect. 7: the independent experimental-numerical comparison confirms the soundness of the contact parameter estimation procedure.

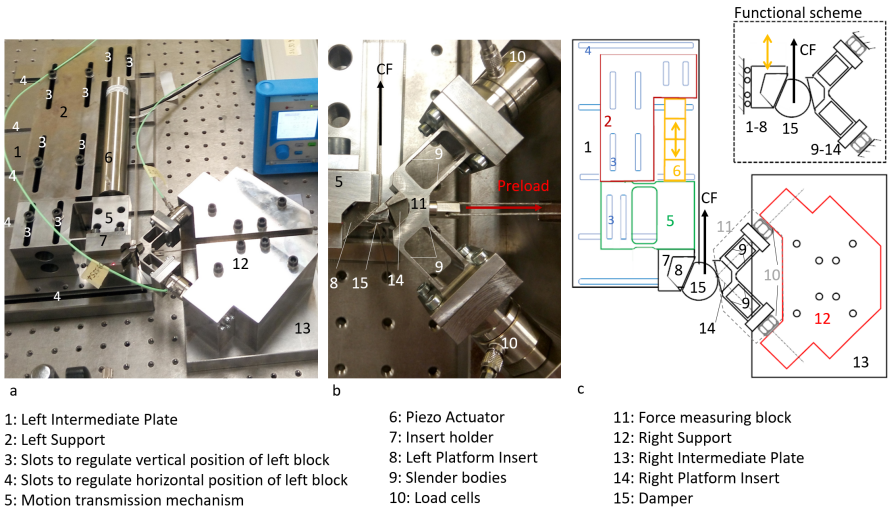

Figure 1: Overview of the test rig and details: (a) picture of the assembled rig (b) close-up picture on the damper and dummy platforms (c) sketch of the main components of the assembled rig and (top right) functional scheme of the rig.

2. Test rig description

The test rig depicted in Fig. 1 is composed of three main parts:,

1. INPUTs: a moving part (13) representing the left blade platform, connected to a piezo-actuator (6) which serves as input motion to the system
2. OUTPUT: a fixed part (main components 8-14) representing the right blade platform, connected to two force sensors (10) which measure the contact forces transmitted between the platforms, through the damper.
3. the interposed under platform damper (15) , held in contact with the platforms by means of a set of wires and pulleys, to reproduce the effect of the centrifugal force.

As shown in the function scheme in Fig. 1c, components 1-8 (left block) provide the input motion to the system, while the goal of components 9-14 is to measure the in-plane contact forces. The test rig is designed to replicate the mechanics of underplatform dampers subjected to blade bending modes, i.e. in-plane

displacements. Torsional modes producing significant out-of-plane platform-damper displacements would require a different experimental set-up. The test rig is capable of reproducing in-plane platform displacements corresponding to the so-called In-Phase (IP: vertical relative motion between the platforms) and Out-of-Phase (OOP: horizontal relative motion) blade bending modes[1], as depicted in Fig. 2. A simple rigid 90° rotation of parts (1)-(6) allows switching from IP to OOP motion. The test rig assembly investigated in the present paper and shown in Fig. 1 is for imposing IP displacements, since this is the blade motion condition closer to the reference cases of interest in service known to the authors. The mechanical components connected to the motion generation and transmission block are: the left intermediate plate (1), the piezo-holder (2) which hosts the piezo-actuator (6) and a mechanism (5) designed to transfer the desired displacement from the piezo stack to the left platform insert (8), connected to (5) by means of the insert holder (7). The piezo holder and the motion transmission mechanism are rigidly connected together and both display vertical slots (3) to adjust the vertical position of the overall left block (components 1 to 8). They are fixed by means of bolts to the left intermediate plate (1), which is equipped with horizontal slots (4) which are used to regulate the horizontal position of the left block with respect to the right block (components 9-14). Component 1 is fixed to the optical table by means of bolts. These vertical and horizontal adjustments allow the rig to host dampers and platform inserts of different dimensions and shape.

The left platform block (5), connected to the motion transmission mechanism, carries the left-platform insert (9), which can be manufactured using different materials and angles to investigate multiple damper-platforms configurations. Parts (5) and (9) are connected by means of bolts: their relative motion has been measured using a differential laser head and found to be negligible (i.e.

[1] Combinations of the two modes of vibration are possible but would require a slight change in the experimental set-up, i.e. with reference to Fig. 1 components n.1 and 7 would have to be re-machined.

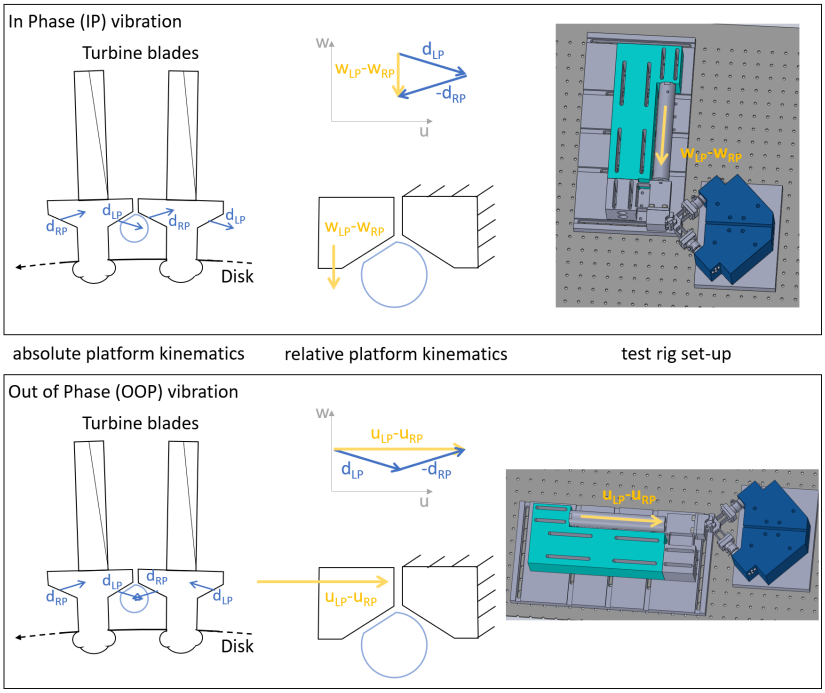

Figure 2: Schematic showing how the absolute platform kinematics (left) in case of IP and OOP motion is transformed into relative platform kinematics (middle) and finally simulated changing the test rig configuration (right).

≤ 0.05 μm.)

Moreover the insert can be equipped with a set of protrusions or tracks, which have a double function. They localize the contact along the damper axis and they ensure the ability to reach high contact pressures using moderate loads on the damper (see also Fig.3).

2.1. Motion transmission mechanism design

Particular attention was paid to the design of the motion transmission mechanism since it has two important functions: transmit the motion without introducing spurious components and protect the piezo from undesirable loads.

A parallel mechanism was chosen due its adequate resolution, low level of parasitic forces, motion smoothness and zero backslash. The parallel mechanism can

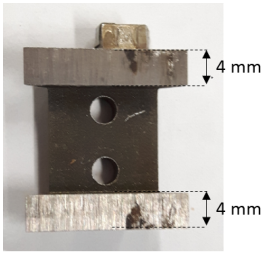

Figure 3: Close-up on one of the platform inserts showing the controlled length tracks and the wear traces on the contact surface.

be seen in Fig. 1a, connecting the fixed part (on the left) and the movable part (on the right) of component (5). Both analytical calculations and FE analysis were used to achieve the required stiffness and keep the additional mass to a minimum. In fact, this is not a resonant rig, and it is therefore desirable to work as far as possible from the rigs internal resonances. If the operating frequency became too close to one of the rigs internal resonances, components of the test rig may start to oscillate polluting the recorded force and displacement signals. According to FE calculations later verified by experimental modal analysis, the first resonant frequency of the rig is set at 779 Hz and sees the motion transmission mechanism bending out of its plane. The experimenter was able to reach up to 550 Hz with a reasonably clean signal. The frequency-limitation is instead set by the piezo actuator, whose performance deteriorates with increasing frequency (practical limit at 350 Hz).

2.2. Force measurement mechanism design

The force measurement device is designed to accurately measure the contact forces acting on the damper. This device is composed of:

- the right-platform insert (14), in contact with the damper (15): it can be manufactured in different shapes (to test different platform angles) and different materials. As in the case of the insert connected to the left platform this insert too can be equipped with protrusions to localize the contact along the damper axis and increase the contact pressure;

- two uniaxial piezoelectric force sensors (10) to measure the in-plane contact forces;
- a device to transmit the load from the right-platform insert to the force sensors (11).

The static component of contact forces and force correction algorithm. Particular care was taken in the selection of the Piezoelectric force sensors. Two Kistler 9323AA load cells were finally chosen for their adequate load range and minimal leakage. In fact, as pointed out in Sect. 3, both the static and dynamic components of the contact forces are essential to correctly estimate friction coefficients. This choice marks a decisive improvement compared to the previous Piezo Damper rig, whose load cells had an inadequate leakage rate, thus making the load removal procedure necessary [51]. The present load cells still suffer from leakage, however the rate is limited ($\approx$ 0.1 mN/sec as measured by the authors) and, most importantly, repeatable and constant in time. This allowed the authors to define a protocol to correct the static component of the force.

The force transmission mechanism. The device to transmit the load to the force sensors, shown in Fig. 1b, is made of two perpendicular slender bodies for each force sensor (9). The slender bodies are stiff along the axial direction and flexible in the transverse direction (axial to transverse stiffness ratio >100). The force sensor at the end of each slender body measures the axial force. This particular geometry was chosen to decouple the two force components, thus avoiding any cross talk, while still ensuring a good performance in the frequency range of interest. A careful parametric study was carried out to select the optimal configuration (i.e. the best trade-off between force decoupling and high-frequency performance). More details about this matter can be found in [26].

3. A sample of results

Each experimental nominal condition - identified by a specific damper, excitation frequency, centrifugal load and direction and amplitude of motion - is investigated through the cross-comparison of a series of quantities (force-related and kinematic).

The force signal at the cylinder-on-flat contact is recorded at each experiment. This signal can be later decomposed into its components (e.g. horizontal and vertical H_R and V_R or tangential and normal to the contact T_R and N_R). Similarly, for each experiment, the flat-on-flat contact force resultant and its position are derived using the damper equilibrium of forces and moments shown in Fig. 4a. Two differential laser heads can be simultaneously applied to measure relevant kinematic quantities, such as the relative platform displacement or the platform-to-damper tangential relative displacement (as in Fig. 4b-c). Further details can be found in [52].

Relevant quantities are then organized into diagrams. The complete list of all observed and derived quantities represented in these diagrams, together with their level of uncertainty, can be found in Table 1.

Two dampers (A and B) are tested within the present experimental campaign. Both of them are curved-flat (see also Fig. 2). Results from Damper A are used as a demonstrator throughout the paper, while Sect. 6 will summarize results coming from both dampers and compare them with results obtained on another curve-flat damper tested on the first Piezo Damper rig. These dampers do not share the same set of platform angles, however they share similar kinematics, i.e. stick-slip with negligible rolling motion, as all of them are pre-optimized [25].

3.1. Testing conditions

The rig in the present configuration simulates a pure In Phase (IP) blade vibration, i.e. the relative motion between adjacent platforms is vertical as in Fig. 2, i.e. a good approximation of EO excitations which produce a reasonably

low (i.e. $< 20°$) inter-blade phase angle. The piezo-electric actuator produces a sinusoidal signal with a given amplitude. The range of amplitude explored within this paper is $\pm$[5-20] μm, the upper limit is defined as the amplitude of motion ensuring the damper reaches bilateral gross slip (condition necessary to estimate friction coefficients).

Results shown here refer to dampers which have undergone a run-in process ($> 7 \cdot 10^6$ cycles before measurement[2]). Furthermore, all results refer to steady state damper behaviour: as already observed in [46] every time an experiment is started, the hysteresis cycles (see Sect. 3.2) rapidly evolve towards a stable and repeatable steady state configuration.

Typical contact pressures for asymmetrical curved-flat dampers range in the 2-4 MPa *nominal* contact pressure at the flat-on-flat contact interface. Corresponding values of force per unit length can be found for the cylinder-on-flat contact interface. This is easily achieved, thanks to the particular shape of the platform inserts (see Fig. 3) using (10-30) kg dead-weights to simulate the centrifugal load. The effect of the centrifugal load on the damper performance is explored in Sect. 3.3.

Important remark: the values indicated above refer to the nominal contact pressure, i.e. assuming that the contact is continuous all along the flat-on-flat contact interface. It will be proven in Sect. 5 that this may not be true, thus leading to non-uniform distribution of contact pressure across the contact interface with local peaks.

Frequencies in the [50-300] Hz have been investigated, further details can be found in Sect. 3.4.

[2]It was observed in [52] that dampers' contact parameters show a larger variability if measured during the initial tests but reach stable and repeatable values within 5-6 million cycles (all recorded values after this point lie scattered within the uncertainty bands). This behaviour has been confirmed in the present case.

Table 1: Essentials in experimental diagrams

Diagram	**Goal**	**Quantities**	**Measurement technique**	**Uncertainty**
OOP Hysteresis	Represent Damper behaviour	$\mathrm{H_R} = \overline{\mathrm{H}}_\mathrm{R} + \Delta\mathrm{H_R}$	Load cells	$2\% \cdot \overline{\mathrm{H}}_\mathrm{R} + 1\% \cdot \Delta\mathrm{H_R}$
		$\mathrm{u_{LP}} - \mathrm{u_{RP}}$	Laser Vibrometer	$0.08\mu m$
IP Hysteresis Fig.5		$\mathrm{V_R} = \overline{\mathrm{V}}_\mathrm{R} + \Delta\mathrm{V_R}$	Load cells	$2\% \cdot \overline{\mathrm{V}}_\mathrm{R} + 1\% \cdot \Delta\mathrm{V_R}$
		$\mathrm{w_{LP}} - \mathrm{w_{RP}}$	Laser Vibrometer	0.08 μm
Hysteresis at the right contact Fig.5-7c	Represent Damper behaviour at the contact, estimate contact stiffness	$T_R = \overline{T}_R + \Delta T_R$	Load cells	$2\% \cdot \overline{\mathrm{T}}_\mathrm{R} + 1\% \cdot \Delta\mathrm{T_R}$
		$\mathrm{t_{RD}} - \mathrm{t_{RP}}$	Laser Vibrometer	0.08 μm
Hysteresis at the left contact Fig.5-7b		$\mathrm{T_L} = \overline{\mathrm{T}}_\mathrm{L} + \Delta\mathrm{T_L}$	Reconstructed	$2\% \cdot \overline{\mathrm{V}}_\mathrm{R} + 1\% \cdot \Delta\mathrm{V_R}$
		$\mathrm{t_{LD}} - \mathrm{t_{LP}}$	Laser Vibrometer	$0.08\mu m$
T/N force ratio Fig.7a	Identify contact states, estimate friction coefficients	T_R/N_R	Load cells	$\approx 3-5\%$
		T_L/N_L	Reconstructed	$\approx 6-10\%$
Right/Left normal contact force vs. time Fig. 8	Identify contact pressure	N_R	Load cells	
		N_L	Reconstructed	
Contact forces diagram Fig. 9b-c	Identify left contact region	T_R, N_R	Load cells	$2\% \cdot \overline{T}_R + 1\% \cdot \Delta\mathrm{T_R}$
		T_L,N_L,application point	Reconstructed	$\approx$ 0.7-0.9 N
Damper rotation vs. time	Kinematic characterization	β (rad)	Laser Vibrometer	$\approx 0.6 \cdot 10^{-4}$ rad $\approx 5\%$

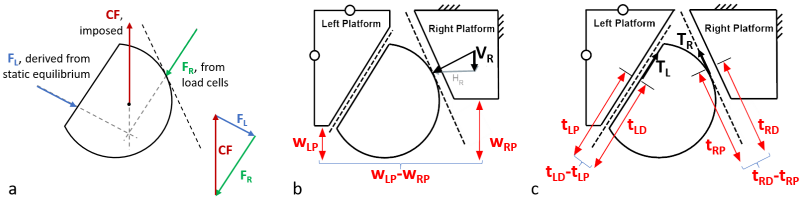

Figure 4: a Scheme representing the right contact force measurement and the derivation of the left contact force resultant. b Schematic of platform-to-platform hysteresis cycle relevant quantities. c Schematic of platform-to-damper (local) hysteresis cycle relevant quantities.

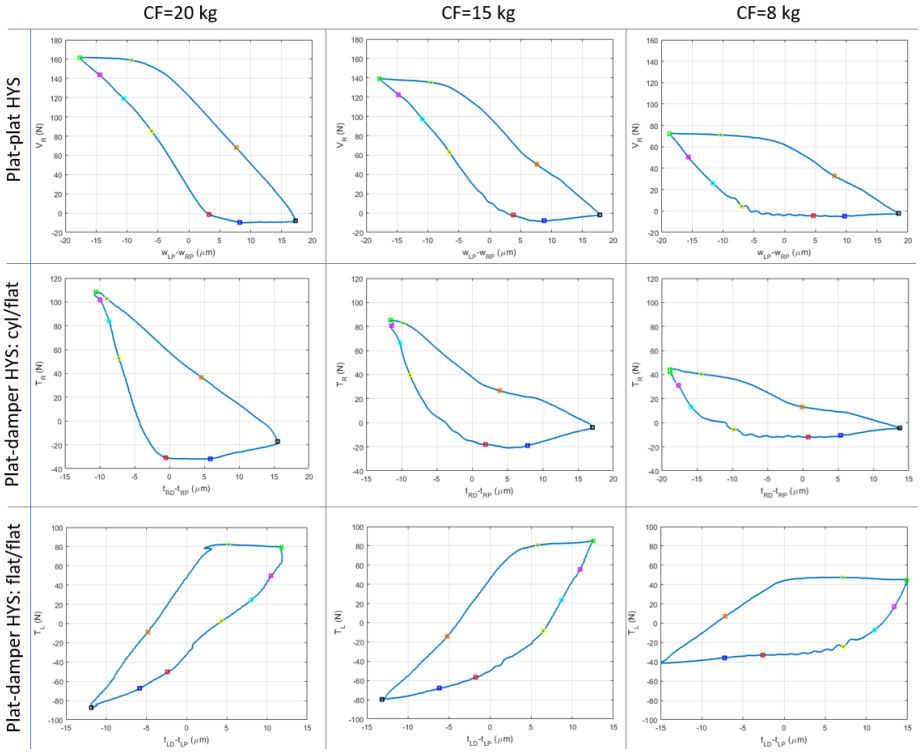

Figure 5: a Platform-to-platform and platform-to-damper hysteresis cycles recorded at f= 100 Hz, centrifugal load CF= [8-20] kg and IP platform-to-platform imposed motion of $\approx \pm 20\mu$m.

3.2. Relevant diagrams

The Platform-to-platform hysteresis cycle is the diagram that best represents the overall damper performance. The platform-to-platform hysteresis diagram is capable of summarizing the effect of the damper between the blades, both in terms of stiffening and of damping effect. The relevant quantities recorded to plot the IP platform-to-platform hysteresis cycle are shown in Fig. 4b. The x axis of the diagrams shows the relative platform motion over one period of vibration. In case of pure In Phase (IP) blade vibration this motion is purely vertical. The y axis of the diagram shows the component of one of the contact forces (either left or right) aligned with the relative platform displacement during one period of vibration. In the IP case the relevant force component is the vertical one, here termed V_R. Three examples of such platform-to-platform hysteresis cycles for increasing centrifugal loads are shown in the first row of Fig. 5 and one for increasing excitation frequencies in Fig. 6a.

The area inside the platform-to-platform hysteresis curve represents the global dissipated energy and its shape given an indication on the damper behaviour[53]. The shape of the cycles in Fig. 5 is regular, typical of a highly efficient stick-slip pattern, compatible with the considerable imposed relative platform motion (i.e. $> \pm 20$ μm).

The platform-to-damper hysteresis cycles are shown in the second and third row of Fig. 5. As described in Tab. 1, they plot the relative displacement at the contact against the corresponding tangential component of the contact force. The relative displacement at the contact is obtained by pointing the laser as described in Fig. 4c. The force is either directly measured ($\mathrm{T_R}$) or obtained derived using the damper static equilibrium ($\mathrm{T_L}$). The platform-to-damper hysteresis cycles will be used in Sect. 4 to estimate tangential contact stiffness values.

Other relevant *force-related quantities can be plotted as a function of time*, as in Fig. 7. They are used to determine contact states at a given instant in time

and, if gross slip is present, to estimate friction coefficient values and estimate pressure at the contact interface (see Sect. 5). Alternatively, forces can be represented as vectors on the damper surface, as shown in Fig. 4a. In detail the left contact force resultant travels along the flat damper-platform surface during the cycle. The position of the left contact force resultant has important consequences on the contact pressure at the flat-on-flat interface (see Sect. 5) and on the overall damper performance. Should the left contact force resultant F_L reach one of the edges of the flat contact surface, that edge will serve as a hinge and the damper will roll (a state known as lift-off), leading to a large damper rotation. Lift-off is very detrimental for the damping efficiency as demonstrated in previous works [25], and makes contact parameter estimation difficult as further commented on in [54]. Thanks to an appropriate selection of the damper cross-section shape and platform angles known as pre-optimization [25], the dampers investigated within this work do not suffer from this condition, therefore their rotation signal is minimal.

3.3. The influence of the centrifugal force

Figure 5 shows the influence of centrifugal load on platform-to-platform and platform-to-damper hysteresis cycles for a 100 Hz 20 μm sinusoidal IP input motion. The shape of the cycles is consistent and so is the damper kinematics (rotation signal not shown for brevity). Considering the first row of Fig. 5 (platform-to-platform hysteresis), it is easy to identify the bilateral gross slip portions of the cycles (i.e. flat segments)[3]. As expected the friction force limit during bilateral gross slip increases with increasing centrifugal loads, i.e. cycles become increasingly "taller". Furthermore, the sliding distance during gross slip (i.e. the length of the fairly flat portion of the cycles) decreases as a larger portion of the period is spent in stick condition. It will be shown in Sect. 4-5 how the centrifugal load changes the contact pressure, thus affecting the contact

[3]The specific contact state of each interface during a specific portion of the cycle is determined as described in Sect. 4.1.

stiffness values.

3.4. The influence of excitation frequency

The comparison of both platform-to-platform and local hysteresis cycles recorded on the same damper at different frequencies (Fig. 6) demonstrates that, at least in the [10-300] Hz range, frequency does not influence neither the damper behavior, and, as further commented on in Sect. 4, nor the contact parameter values.

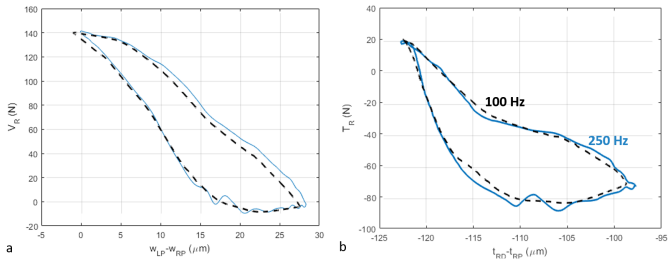

Figure 6: Comparison of 100 Hz and 250 Hz : a. Platform-to-platform and b. Platform-to damper hysteresis cycles obtained at CF=15 kg.

4. Estimation of contact parameters

One of the main goals of the present rig is to estimate contact parameters to be fed to a numerical model of the UPD within a set of platforms, such as the one described in [55]. The damper numerical model requires a description of the friction interface: the authors chose a state-of-the-art 2D macroslip contact element[10], whose calibration parameters are normal and tangential contact stiffness, here termed k_n and k_t and friction coefficient μ. One contact element is used to represent the cylinder-on-flat contact, while the flat-on-flat contact requires a minimum of two contact elements. As a result two sets of contact

parameters have to be determined, one for each contact interface[4].

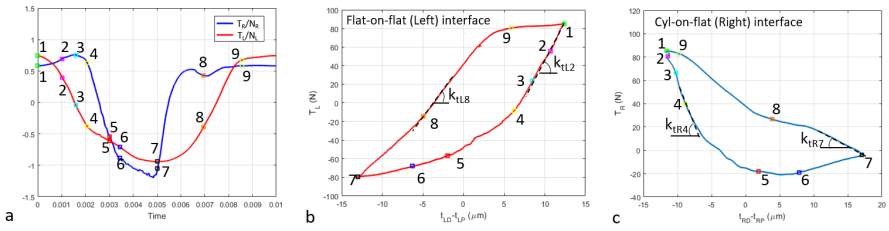

Figure 7: a.T/N force ratio b. local (cylinder on flat) hysteresis c. local (flat on flat) hysteresis for CF= 15 kg, f= 100 Hz, imposed platform motion 20 μm

4.1. Friction coefficients

The damper contact states during one period of vibration are estimated through the ratio of the total tangential and normal force components on the left and right contact surfaces plotted as a function of time. An example can be found in Fig. 7a. Relevant points on the T/N diagram can be marked by a symbol and a number. These points represent relevant transition of contact states happening during the period of vibration. They are marked on the other diagrams as well, thus serving as a reference.

The flat portions of each T/N line may indicate a slip phase on an interface - subject to cross-confirmation by other diagrams (i.e. Fig. 7b-c). As an example the flat-on-flat T_L/N_L force ratio is approximately flat from stage 9 to 1: the corresponding hysteresis cycle in Fig. 7b confirms the gross slip assumption since the damper-platform relative motion during that same stage is considerable (> 7 μm). In such cases the ratio T/N will represent a friction coefficient under the assumption of classical Coulomb friction with a constant friction coefficient. Conversely, if the T/N force ratio is changing in time then that interface will be in stick condition.

[4]It is here assumed that all contact elements used to represent the flat-on-flat contact share the same contact parameters.

The analysis of the T/N force ratio diagram in Fig. 7a allows identifying the gross slip stages, i.e. 6-7 and 9-1. The corresponding T/N force ratio signals during those stages are:

- Left interface(flat-on-flat): $T/N_{6-7} \approx 0.7 - 0.9$ and $T/N_{9-1} \approx 0.75$;
- Right interface (cylinder-on-flat): $T/N_{6-7} \approx 0.85 - 1.1$ and $T/N_{9-1} \approx 0.6$;

These ratios can be considered friction coefficients since the associated damper-to-platform relative displacement is non-negligible (see local hysteresis cycles in Fig. 7b-c). It can be concluded that:

- The friction coefficient at the flat-on flat interface μ_L ranges between 0.7 and 0.85, the slight difference between the two stages may be due to a variety of factors (velocity at the contact, local surface condition, varying normal load during sliding) and similar variability has been encountered throughout the experimental campaign.
- The friction coefficient at the cylinder-on-flat interface μ_R ranges between 0.6 and 0.75. Higher values evidenced at the end of stage 6-7 should not be trusted as the corresponding normal contact force N_R (see Fig. 8) reaches very low values, thus introducing a larger uncertainty in the T/N values.

Friction coefficients vary during the sliding phase and can be different in the two sliding directions. The variation during sliding may be due to the fact that during the particular stage of gross slip (6-7), the normal load is varying continuously. This may in turn change the local contact conditions during sliding and therefore produce a variation of friction coefficient. As for the difference in sliding in the two directions it may be due to a variety of factors (different normal load during the different portions of the cycle, higher uncertainty due to low normal load) and/or different local surface conditions. The procedure described above has been repeated for two different curved-flat dampers of the same material and dimension and for different experimental nominal conditions (i.e. centrifugal load and frequency in the ranges discussed in sect. 3). Results

are repeatable, all measured friction coefficients stay in the [0.6-0.8] range, with some dispersion (σ^2 in the [0.05-0.06] range for both interfaces) has been observed. This moderate variability is not linked, to the authors knowledge, to a specific change in experimental conditions as no clear trend could be observed. These results cross-confirm previous findings on similar dampers [56, 48] tested using the first Piezo Damper Rig.

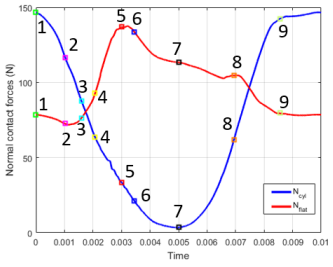

Figure 8: Normal contact forces in time for CF= 15 kg, f= 100 Hz, imposed platform motion 20 μm

4.2. Contact stiffness values

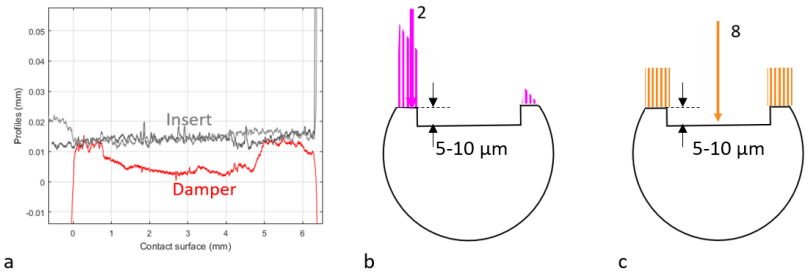

Figure 9: a Profile. b-c Representation of normal contact force and resulting contact pressure at the flat-on-flat interface during selected stages (stages 2 and 8) of the period of vibration for for CF= 15 kg, f= 100 Hz, imposed platform motion 20 μm

Normal contact stiffness can be found in the literature for cylinder-on-flat contacts[57, 58], while the stiffness related to flat-on-flat contacts is trickier

to estimate, as shown in [28]. Fortunately, in the authors' experience, normal contact stiffness tends to be higher than the corresponding tangential stiffness. As a result, their specific values have a negligible influence on the FRF and damper behaviour, i.e. it is the weaker (tangential) spring which "counts", as demonstrated in [49].

For all these reasons this paper focuses on the direct estimation of tangential contact stiffness values of non rolling cylinder-on-flat and flat-on-flat contacts. To this purpose, as shown in Fig. 7b-c, local (i.e. tangential) hysteresis cycles are used to relate the tangential component of a contact force (T_R or T_L) to the corresponding relative damper-platform displacement ($t_{RD} - t_{RP}$ or $t_{LD} - t_{LP}$). A specific procedure has been developed to estimate tangential contact stiffness values and relate them to the contact pressure:

- As descried previously, the period of vibration is divided into stages, marked by a symbol and a number. The portions of the cycle corresponding to a stick state are identified by selecting the portions of the cycle with a T/N ratio varying in time (see Fig. 7a), e..g stages 4-5 and 7-8 for the cylinder-on-flat interface.

- The corresponding portions of the cycle are identified on the local hysteresis cycle (i.e. Fig. 7b-c), the slope of the local hysteresis cycle close to that stage corresponds to the interface.

The procedure described above yields as many k_t estimates at the stick contact states identified on the T/N diagram. In the present case k_{tR4} and k_{tR7} for the cylinder on flat interface and k_{tL2} and k_{tL8} for the flat-on-flat interface highlighted in Fig. 7b-c. The reader will notice that $k_{tR4} \neq k_{tR7}$ and $k_{tL2} \neq k_{tL8}$. It will be shown in the following section how these differences are linked to the actual pressure at the contact interface.

5. Contact pressure

Contact pressure can be defined with increasing accuracy levels:

1. the centrifugal load produces a "nominal mean" value of normal load and therefore of contact pressure, both at the cylinder-on-flat and flat-on-flat contact;
2. this mean value may vary in time due to the harmonic component of the contact forces;
3. finally, in the case of conforming contacts (i.e. flat-on-flat) the pressure distribution may change depending on the position of the left contact force resultant and to the specific configuration of the mating surfaces (platform-damper).

The purpose of this section is to show how inadequate "nominal contact pressure" concept (point 1 of the list above) is and to propose a more refined alternative. This last task is performed differently depending on the geometry of the contact. In the case of the cylinder-on-flat contact interface (k_{tR}) it is sufficient to look at the value of the normal contact force during that stage as the contact is non-conforming (see Fig. 8), i.e. point 2 of the list above is enough. As expected, higher values of contact stiffness are found at stages where the normal contact force is higher (i.e. $k_{tR4} > k_{tR7}$ since $N_{R4} > N_{R7}$).

In the case of the flat-on-flat contact interface (k_{tL}), the normal contact force value as well as its position and the contact interface configuration play an important role. For this reason the configuration of damper and platform were scanned using a profilometer at multiple locations along the damper axial length. The resulting profiles were found to be very repeatable, a sample of which is reported in Fig. 9a. It can be observed that the flat-on-flat contact is far from continuous, two protrusions can be observed at the outer edges of the damper. The effective width of the contact area is definitely smaller than the nominal one ($\approx$ 2.5 mm vs. 6.3 mm). This has obvious consequences on the contact pressure values, which become larger than the expected "nominal" values.

As a first hand approximation is it possible to assume a linear distribution of contact pressure and therefore sketch the contact pressure on the flat contact interface during the stages (see Fig. 7b-c) used to estimate k_{tR} and k_{tL}. The

linear distribution of contact pressure assumption will fail to catch very local effects (i.e. local sharp peaks at the edges of the contact), but will give an adequate estimate of the mean pressure on each protrusion during stages 2 and 8.

It can be observed that $k_{tL2} > k_{tL8}$ despite the fact that the normal contact force at stage 2 is slightly lower than that at stage 8. However, in this specific case, at stage 2 the contact force lies on one of the pads that constitute the flat interface, thus yielding a very high and localized contact pressure (see Fig. 9b). On the other hand, at stage 8, the contact force resultant is between the two pads, thus yielding a uniform (and lower) contact pressure (see Fig. 9c). Once again it is observed that tangential contact stiffness values increase with increasing contact pressure.

6. Contact stiffness values: a summary of results

Tangential contact stiffness at the cylinder-on-flat and flat-on-flat interface has been here measured for two sets of curved-flat dampers sharing the same material and dimension but slightly different platform angles. The experimental campaign saw increasing values of centrifugal load (CF), different amplitudes of motion and frequency of excitation. However only the centrifugal load (i.e. linked to contact pressure) had a significant effect on the contact stiffness values: the dependence of contact stiffness on the effective mean pressure at the contact is here investigated. As described above, tangential relative displacements are measured directly and related to the corresponding tangential contact force. As further commented on in [54], this technique is applicable only if the contact is not rolling.

Cylinder-on-flat interface. In all cases the cylinder-on-flat tangential contact stiffness, computed for a controlled length of contact of 8 mm, is related to the linear contact pressure (normal load N_R per unit length). It was here chosen not to apply Hertz theory to compute the contact area and therefore the contact pressure because the main goal is to provide the designer with straightforward

information (i.e. directly linked to the centrifugal load). The results are reported in Fig. 10a. The error bars are obtained as described in Appendix A. Results for the different dampers are consistent (i.e. different dampers show similar k_t values provided the contact pressure is in the same range) and show a positive dependence on the contact pressure, as already observed in [59].

Flat-on-flat interface. In all cases the flat-on-flat tangential contact stiffness is computed for a controlled axial length of contact of 8 mm. Given the results evidenced in Sect. 5, the width of contact is estimated directly using a profilometer for all investigated dampers. In all cases the tangential contact stiffness is related to the contact pressure, obtained considering both the magnitude of the normal force resultant and its position. The results are reported in Fig. 10b. As in the previous case, the contact stiffness increases with contact pressure.
An additional comparison is performed using results on a curved-flat damper already presented in [52] and tested on the first Piezo Damper Rig for a limited centrifugal load range. Once again the effective mean value of contact pressure is estimated using the combined experimental results from profilometer and contact force amplitude and position, as described in Sect. 4-5.
Results for the three different curved-flat dampers (measured on two different rigs) are remarkably consistent. This consistency is the result of the careful consideration of the effective loading conditions of the flat-on-flat contact surfaces during the different stages of the cycle. It is worth noticing that if the contact stiffness values had been plotted against the "nominal" contact pressure no clear trend would have been observed.

7. Numerical simulation

The effectiveness of the contact parameter estimation procedure is tested by feeding the parameters to a damper simulation tool already presented in [25, 60]. The numerical tool will produce hysteresis cycles which will be compared ex-post with their experimental counterpart. The sole inputs to the code are:

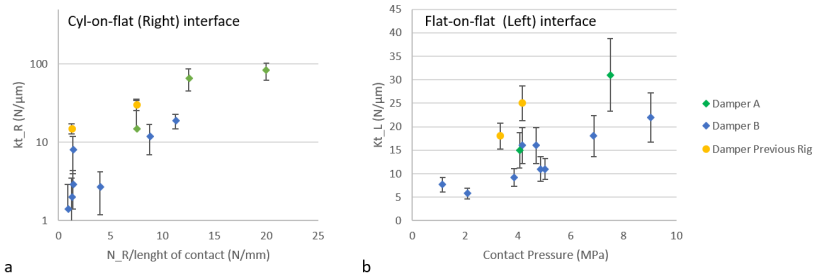

Figure 10: a. Tangential contact stiffness at the cylinder-on-flat interface as a function of the effective mean "linear" contact pressure. b. Tangential contact stiffness at the flat-on-flat interface as a function of the mean effective contact pressure.

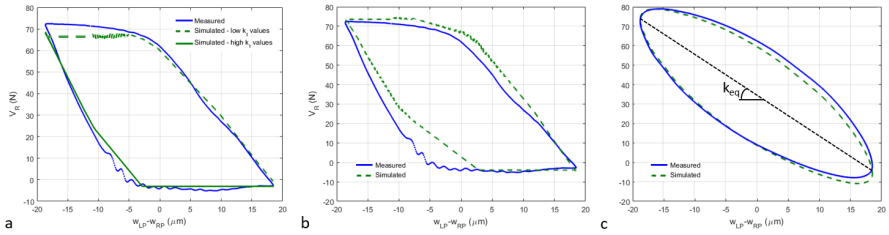

Figure 11: Measured vs. Simulated platform-to-platform hysteresis cycle for CF= 8kg, f=100 Hz, 20 μm imposed motion. Numerical result obtained with a. normal load-dependent b. constant tangential contact stiffness. c. HBM equivalent of the cycles in Fig. 11b.

- mass and inertia properties of the damper (the damper is simulated as a rigid body);
- position of the selected contact nodes with respect to the damper center of mass;
- experimental conditions, i.e. frequency, centrifugal force, recorded relative platform motion signal;
- contact parameter values from Sect. 4.

The damper equilibrium equations can be solved either using HBM as in [25] or the time-marching technique developed in [60]. No other assumption or fine

tuning technique is here applied. The resulting hysteresis cycle and damper kinematics are compared to their experimental counterpart. It should be noted that the platform-to-platform hysteresis cycle, not used to estimate contact parameters, is here used solely as validation data. Furthermore, unlike platform-to-damper cycles, it provides a synthetic representation of the overall damper effect on the blades (the ultimate goal of the present investigation). The slopes of the stick portion of the cycle are linear combination of the contact stiffness values, while the upper and lower force limits (flat portions of the cycle) are influenced by the friction coefficient values.

As evidenced in Sect. 6 contact stiffness values can undergo changes even during a single period of vibration. This, in principle, can be accommodated inside the damper numerical model. The result of such choice is shown in Fig. 11a. The shape similarity is remarkable, with an area which is only 4% smaller than the measured one.

On the other hand, the damper numerical model should be seen as a design tool and, as such, it should be easy and quick to use. It is acceptable and necessary to update contact stiffness values depending on the centrifugal load. It may not be practical however, to have to change the contact stiffness values during a period of vibration. A second simulation was run using mean values of contact stiffness, i.e. with reference to Fig. 7b-c $k_{tR4} < k_{tR} < k_{tR8}$ and $k_{tL8} < k_{tL} < k_{tL2}$. The result is shown in Fig. 11b. The shape similarity has diminished, but the area is approximately unchanged. Furthermore, if the harmonic balance equivalent of the cycle [5] is considered (see Fig. 11c), the differences become truly negligible. The effect of the contact stiffness values on the hysteresis cycle changes with the amplitude of platform-to-platform motion. The case shown in Fig. 11 displays a moderate amount of bilateral gross slip and has been chosen purposely as a demonstrator. Should the amplitude of motion be larger, than the effect of the contact stiffness on the overall area of the cycle would decrease as demonstrated in [61].

[5] first harmonic of displacement vs. first harmonic of the force

Similarly, the choice of keeping the friction coefficients constant throughout the period of vibration, despite the slight asymmetry evidenced in Sect. 4.1, does produce a simulated platform-to-platform cycle slightly taller than its measured counterpart. Nevertheless, these differences are deemed acceptable as the simulated HBM equivalent of the platform-to-platform hysteresis cycle (i.e. the effect on the blades) differs from the measured counterpart by less than 5% on equivalent stiffness (see Fig. 11c) and 3% on equivalent damping (i.e. the area of the cycle).

8. Conclusions

This paper presents a novel test rig for the direct experimental investigation of the mechanics of underplatform dampers under realistic experimental conditions in terms of frequencies and nominal contact pressures. The experimental results are here used to estimate tangential contact stiffness and friction coefficient values to be fed to a damper-blades numerical model. The following observations can be drawn from the results analysis:

- frequency does not affect contact parameter values in the investigated range 10-300 Hz;
- friction coefficient values are repeatable, affected by a moderate dispersion;
- measured contact stiffness values are influenced by the contact pressure, or normal load per unit length in the case of cylinder-on-flat interfaces.

Measured contact stiffness values from different dampers are remarkably repeatable and consistent, provided that the effective contact pressure is recorded. If flat-on-flat interfaces are concerned, the nominal contact pressure (i.e. mean value of normal load over nominal contact area) should be substituted with the mean effective contact pressure concept, taking into account the value of normal load at a given instant in time, its position over the surface and the interface morphology. This finding proves that mapping contact parameter values is indeed possible, however predicting the contact stiffness of an interface without

specific information over its morphology does introduce a large degree of uncertainty.

The effectiveness of the contact parameter estimation procedure is further confirmed by the comparison of the present set of results with those found on similar dampers on a previous Piezo Damper rig.

The contact parameters thus derived are fed to a state-of-the-art damper numerical model. The ensuing experimental-numerical comparison confirms that the contact parameter estimate allows reconstructing platform-to-platform hysteresis cycles simply starting from the relative motion of the platforms.

Acknowledgments

The construction of the test rig presented in this paper has been funded within a research contract supported by Ansaldo Energia s.p.a.

Appendix A. Remark on uncertainty of tangential contact stiffness results

Measurement uncertainty (derived from instruments specs and error propagation techniques) is quite low. In fact, the tangential contact stiffness is defined as the ratio of a variation of the contact force over a variation of displacement. This kind of procedure rids the measurement of the most common forms of bias if the calibration factors are known accurately. A much larger source of uncertainty is instead introduced by the data processing technique. In fact, results change depending on the selected portion of curve.

Although a procedure has been devised in order to standardize the selection process, this variability is still critical. In order to take this effect into account a linear least square fitting is performed. This procedure gives two important pieces of information:

- the R^2 coefficient, a measure of the goodness of the fit, i.e. the fraction of the variability of the experimental data accounted for by the linear model;

- the slope of the fitted line together with its standard deviation.

When the model is a very good fit, there is little deviation between the data and the model: in this case it holds $R^2 1$. The investigated cases display R^2 values always above 0.92. The standard deviation is represented in Fig. 10 using error bars.

References

[1] B. D. Yang, J. J. Chen, C. H. Menq, Prediction of resonant response of shrouded blades with three-dimensional shroud constraint, Journal of Engineering for Gas Turbines and Power 121 (3) (1999) 523. doi:10.1115/1.2818504.

[2] S. Yajie, H. Jie, S. Yingchun, Z. Zigen, Forced response analysis of shrouded blades by an alternating frequency/time domain method, in: Volume 5: Marine Microturbines and Small Turbomachinery Oil and Gas Applications Structures and Dynamics, Parts A and B, ASME, 2006. doi:10.1115/gt2006-90595.

[3] J. Szwedowicz, C. Gibert, T. P. Sommer, R. Kellerer, Numerical and experimental damping assessment of a thin-walled friction damper in the rotating setup with high pressure turbine blades, ASME. J. Eng. Gas Turbines Power 130 (1) (2008) 012502–012502–10. doi:10.1115/1.2771240.

[4] C. Siewert, L. Panning, J. Wallaschek, C. Richter, Multiharmonic forced response analysis of a turbine blading coupled by nonlinear contact forces, Journal of Engineering for Gas Turbines and Power 132 (8) (2010) 082501. doi:10.1115/1.4000266.

[5] S. Zucca, C. M. Firrone, M. M. Gola, Numerical assessment of friction damping at turbine blade root joints by simultaneous calculation of the static and dynamic contact loads, Nonlinear Dynamics 67 (3) (2011) 1943–1955. doi:10.1007/s11071-011-0119-y.

[6] W. Gu, Z. Xu, Y. Liu, A method to predict the non-linear vibratory response of bladed disc system with shrouded dampers, Proceedings of the Institution of Mechanical Engineers, Part C: Journal of Mechanical Engineering Science 226 (6) (2011) 1620–1632. doi:10.1177/0954406211424671.

[7] M. Mitra, S. Zucca, B. Epureanu, Adaptive microslip projection for reduction of frictional and contact nonlinearities in shrouded blisks, Journal of Computational and Nonlinear Dynamics 11 (4) (2016) 041016. doi:10.1115/1.4033003.

[8] S. M. Pourkiaee, S. Zucca, A reduced order model for nonlinear dynamics of mistuned bladed disks with shroud friction contacts, in: Volume 7C: Structures and Dynamics, ASME, 2018. doi:10.1115/gt2018-75223.

[9] A. Hartung, H.-P. Hackenberg, M. Krack, J. Gross, T. Heinze, L. P. von Scheidt, Rig and engine validation of the non-linear forced response analysis performed by the tool OrAgL, in: Volume 7C: Structures and Dynamics, ASME, 2018. doi:10.1115/gt2018-75186.

[10] B. Yang, M. C.H., Characterization of contact kinematics and application to the design of wedge dampers in turbomachinery blading: Part 2 – prediction of forced response and experimental verification., ASME J. Eng. Gas Turbines Power 120 (2) (1998) 418–423. doi:10.1115/1.2818139.

[11] L. Panning, W. Sextro, K. Popp, Optimization of interblade friction damper design, in: Volume 4: Manufacturing Materials and Metallurgy Ceramics Structures and Dynamics Controls, Diagnostics and Instrumentation Education, ASME, 2000. doi:10.1115/2000-GT-0541.

[12] L. Panning, W. Sextro, K. Popp, Spatial dynamics of tuned and mistuned bladed disks with cylindrical and wedge-shaped friction dampers, International Journal of Rotating Machinery 9 (3) (2003) 219–228. doi:10.1155/S1023621X03000198.

[13] E. P. Petrov, D. J. Ewins, Advanced modeling of underplatform friction dampers for analysis of bladed disk vibration, Journal of Turbomachinery 129 (1) (2007) 143. doi:10.1115/1.2372775.

[14] T. Berruti, C. Firrone, M. Pizzolante, M. Gola, Fatigue damage prevention on turbine blades: Study of underplatform damper shape, Key Eng Mat 347 (2007) 159–164. doi:10.4028/www.scientific.net/KEM.347.159.

[15] T. Berruti, A test rig for the investigation of the dynamic response of a bladed disk with underplatform dampers, Mech. Re.Commun. 37 (6) (2010) 581–583. doi:10.1016/j.mechrescom.2010.07.008.

[16] I. Sever, P. E.P., E. D.J., Experimental and numerical investigation of rotating bladed disk forced response using underplatform friction dampers, ASME J. Eng. Gas Turbines Power 130 (4) (2008) 042503–11. doi:10.1115/1.2903845.

[17] C. M. Firrone, T. M. Berruti, M. M. Gola, On force control of an engine order–type excitation applied to a bladed disk with underplatform dampers, Journal of Vibration and Acoustics 135 (4) (2013) 041103. doi:10.1115/1.4023899.

[18] D. Botto, C. Gastadi, M. M. Gola, M. Umer, An experimental investigation of the dynamics of a blade with two under-platform dampers, Journal of Engineering for Gas Turbines and Power 140 (3) (2017) 032504. doi:10.1115/1.4037865.

[19] L. Pesaresi, L. Salles, A. Jones, J. Green, C. Schwingshackl, Modelling the nonlinear behaviour of an underplatform damper test rig for turbine applications, Mechanical Systems and Signal Processing 85 (2017) 662–679.

[20] K. Šanliturk, D. Ewins, A. Stanbridge, Underplatform dampers for turbine blades: theoretical modelling, analysis and comparison with experimental data, J Eng Gas Turbine Power 123 (4) (2001) 919–929.

[21] L. Panning, K. Popp, W. Sextro, F. Götting, A. Kayser, I. Wolter, Asymmetrical underplatform dampers in gas turbine bladings: Theory and applicationdoi:10.1115/GT2004-53316.

[22] S. Zucca, J. Borrajo, M. Gola, Forced response of bladed disks in cyclic symmetry with underplatform dampers, in: Volume 5: Marine Microturbines and Small Turbomachinery Oil and Gas Applications Structures and Dynamics, Parts A and B, ASME, 2006. doi:10.1115/GT2006-90785.

[23] K.-H. Koh, J. H. Griffin, Dynamic behavior of spherical friction dampers and its implication to damper contact stiffness, Journal of Engineering for Gas Turbines and Power 129 (2) (2007) 511. doi:10.1115/1.2436547.

[24] T. Berruti, C. Firrone, M. Gola, A test rig for noncontact traveling wave excitation of a bladed disk with underplatform dampers, Journal of Engineering for Gas Turbines and Power 133 (2011) 1–7.

[25] C. Gastaldi, T. M. Berruti, M. M. Gola, Best practices for underplatform damper designers, Proceedings of the Institution of Mechanical Engineers, Part C: Journal of Mechanical Engineering Science 232 (7) (2018) 1221–1235. doi:10.1177/0954406217753654.

[26] D. Botto, M. Umer, A novel test rig to investigate under-platform damper dynamics, Mechanical Systems and Signal Processing 100 (2018) 344–359.

[27] M. Hls, L. P. von Scheidt, J. Wallaschek, Influence of geometric design parameters onto vibratory response and HCF safety for turbine blades with friction damper, in: Volume 7C: Structures and Dynamics, ASME, 2018. doi:10.1115/gt2018-75363.

[28] C. Gastaldi, M. M. Gola, Criteria for best performance of pre-optimized solid dampers, in: ASME Turbo Expo 2018 Volume 7C: Structures and Dynamics, ASME, 2018. doi:10.1115/gt2018-75961.

[29] M. Afzal, I. L. Arteaga, L. Kari, An analytical calculation of the jacobian matrix for 3d friction contact model applied to turbine blade shroud

contact, Computers & Structures 177 (2016) 204–217. doi:10.1016/j.compstruc.2016.08.014.

[30] C. Gastaldi, A. Fantetti, T. Berruti, Forced response prediction of turbine blades with flexible dampers: The impact of engineering modelling choices, Applied Sciences 8 (1) (2017) 34. doi:10.3390/app8010034.

[31] A. Fantetti, C. Gastaldi, T. Berruti, Modeling and testing friction flexible dampers: Challenges and peculiarities, Experimental Techniques 42 (4) (2018) 407–419. doi:10.1007/s40799-018-0248-z.

[32] J. Griffin, Friction damping of resonant stresses in gas turbine engine airfoils, Journal of Engineering for Power 102 (2) (1980) 329. doi:10.1115/1.3230256.

[33] K.-H. Koh, J. H. Griffin, S. Filippi, A. Akay, Characterization of turbine blade friction dampers, Journal of Engineering for Gas Turbines and Power 127 (4) (2005) 856. doi:10.1115/1.1926312.

[34] D. Botto, M. Lavella, M. M. Gola, Measurement of contact parameters of flat on flat contact surfaces at high temperature, in: Volume 7: Structures and Dynamics, Parts A and B, ASME International, 2012.

[35] K. Y. Sanliturk, A. B. Stanbridge, D. J. Ewins, Friction dampers: measurement, modelling and application to blade vibration control, in: N. Y. ASME (Ed.), Proc. Des. Eng. Conf. , Vol. 3, Part B, Vol. 84, 1995, pp. 1377 – 1382.

[36] S. Filippi, A. Akay, M. Gola, Measurements of tangential contact hysteresis during microslip, Journal of Tribology 126 (2004) 482–489.

[37] C. Schwingshackl, E. Petrov, E. D.J., Validation of test rig measurements and prediction tools for friction interface modelling, in: N. Y. ASME (Ed.), Turbo Expo: Power for Land, Sea, and Air, Vol. 6, 2010. doi:10.1115/GT2010-23274.

[38] C. Firrone, Measurement of the kinematics of two underplatform dampers with different geometry and comparison with numerical simulation, Journal of Sound and Vibration 323 (1-2) (2009) 313–333. doi:10.1016/j.jsv.2008.12.019.

[39] J. Szwedowicz, M. Kissel, B. Ravindra, R. Kellerer, Estimation of contact stiffness and its role in the design of a friction damper, in: Volume 4: Manufacturing Materials and Metallurgy Ceramics Structures and Dynamics Controls, Diagnostics and Instrumentation Education IGTI Scholar Award, ASME, 2001. doi:10.1115/2001-GT-0290.

[40] W. Sextro, K. Popp, I. Wolter, Improved reliability of bladed disks due to friction dampers, in: ASME. Turbo Expo: Power for Land, Sea, and Air, Vol. 4 of Manufacturing Materials and Metallurgy, 1997. doi:10.1115/97-GT-189.

[41] K. Y. Sanliturk, D. J. Ewins, A. B. Stanbridge, Underplatform dampers for turbine blades: Theoretical modeling, analysis, and comparison with experimental data, ASME. J. Eng. Gas Turbines Power 123 (1998) 919 – 929. doi:10.1115/1.1385830.

[42] A. Bessone, F. Toso, T. Berruti, Investigation on the dynamic response of blades with asymmetric under platform dampers, ASME Turbo Expo 7B (GT2015-42597). doi:10.1115/GT2015-42597.

[43] B. Yang, M. Chu, C. Menq, Stick-slip-separation analysis and non-linear stiffness and damping characterization of friction contacts having variable normal load, Journal of Sound and Vibration 210 (4) (1998) 461–481. doi:10.1006/jsvi.1997.1305.

[44] E. Cigeroglu, N. An, C. H. Menq, Forced response prediction of constrained and unconstrained structures coupled through frictional contacts, ASME J. Eng. Gas Turbines Power 131 (2) (2009) 022505–022505–11. doi:10.1115/1.2940356.

[45] J. Szwedowicz, T. Secall-Wimmel, P. Dünck-Kerst, Damping performance of axial turbine stages with loosely assembled friction bolts: The nonlinear dynamic assessment, Journal of Engineering for Gas Turbines and Power 130 (3) (2008) 032505. doi:10.1115/1.2838998.

[46] M. M. Gola, T. Liu, A direct experimental-numerical method for investigations of a laboratory under-platform damper behavior, International Journal of Solids and Structures 51 (25-26) (2014) 4245–4259.

[47] M. Gola, C. Gastaldi, Understanding complexities in underplatform damper mechanics, in: Volume 7A: Structures and Dynamics, ASME International, 2014. doi:10.1115/GT2014-25240.

[48] C. Gastaldi, M. Gola, Pre-optimization of asymmetrical underplatform dampers, Journal of Engineering for Gas Turbines and Power 139 (GTP-16-1229) (2016) 012504. doi:10.1115/1.4034191.

[49] C. Gastaldi, M. Gola, Estimation accuracy vs. engineering significance of contact parameters for solid dampers, no. 1, 2017, pp. 1–8.

[50] M. Gola, M. B. D. Santos, T. Liu, Design of a new test rig to evaluate underplatform damper performance, in: ESDA 2010 - 24268, 2010.

[51] M. M. Gola, M. Bragas Dos Santos, T. Liu, Measurement of the scatter of underplatform damper hysteresis cycle: experimental approach, in: Proc. of ASME IDETC, DETC2012-70269, 2012, pp. 359–369.

[52] C. Gastaldi, Vibration control and mitigation in turbomachinerydoi:10.6092/polito/porto/2677053.

[53] C. Gastaldi, M. M. Gola, Pre-optimization of asymmetrical underplatform dampers, in: Volume 7A: Structures and Dynamics, ASME, 2016. doi:10.1115/gt2016-57359.

[54] C. Gastaldi, T. M. Berruti, M. M. Gola, A. Bessone, Experimental investigation on real under-platform dampers: the impact of design and manufacturing, in: Proceedings of ASME Turbo Expo 2019.

[55] C. Gastaldi, T. M. Berruti, M. M. Gola, The relevance of damper pre-optimization and its effectiveness on the forced response of blades, in: Proc. ASME Turbo Expo 2017, GT2017-64402, Charlotte, NC, USA, 2017.

[56] C. Gastaldi, M. M. Gola, Testing, simulating and understanding underplatform damper dynamics, in: Proceedings of the VII European Congress on Computational Methods in Applied Sciences and Engineering (ECCOMAS Congress 2016), 2016. doi:10.7712/100016.2134.11184.

[57] J. Brändlein, P. Eschmann, L. Hasbargen, K. Ball, Ball and Roller Bearings: Theory, Design, and Application, 3rd Edition, John Wiley and Sons, ISBN: 0471984523, 1999.

[58] T. . Harris, M. Kotzalas, Rolling Bearing Analysis, 5th Edition, CRC Press, ISBN: 0849381673, 2006.

[59] M. Kartal, D. Mulvihill, D. Nowell, D. Hills, Measurements of pressure and area dependent tangential contact stiffness between rough surfaces using digital image correlation, Tribology International 44 (10) (2011) 1188–1198. doi:10.1016/j.triboint.2011.05.025.

[60] C. Gastaldi, T. Berruti, Competitive time marching solution methods for systems with friction-induced nonlinearities, Applied Sciences 8 (2) (2018) 291. doi:10.3390/app8020291.

[61] C. Gastaldi, M. Gola, On the relevance of a microslip contact model for under-platform dampers, International Journal of Mechanical Sciences 115-116 (2016) 145–156. doi:http://dx.doi.org/10.1016/j.ijmecsci.2016.06.015.